Short-term effects of impurities in the CO_2 stream injected into fractured carbonates

J.C. de Dios[a,*], M.A. Delgado[a], J.A. Marín[a], C. Martinez[b], A. Ramos[b], I. Salvador[a], L. Valle[c]

[a] *Fundación Ciudad de la Energía, Av. del Presidente Rodríguez Zapatero, s/n, Cubillos del Sil, León 24492, Spain*
[b] *Technical University of Madrid, School of Mines and Energy, c/de Ríos Rosas 21, Madrid 28003, Spain*
[c] *Fundación Instituto Petrofísico, c/Eric Kandel 1, 28906 Getafe, Madrid, Spain*

A B S T R A C T

After the Paris Agreement in which 195 countries are involved, the Carbon Capture and Storage (CCS) is now an accepted technology in the United Nations Framework Convention on Climate Change (UNFCCC). In Spain, *Fundación Ciudad de la Energía* (CIUDEN) has successfully completed the full CCS chain, being CO_2 captured in the Technology Development Centre in *Cubillos del Sil* (*León*, Spain) whereas that it is geologically stored in a deep saline aquifer, formed by fractured carbonates with poor matrix porosity, located in the Technology Development Plant (TDP) at Hontomín (Burgos, Spain).

The results of the field tests, in which up to 150 t of CO_2 and synthetic air (5%v of N_2 and O_2) were co-injected on site, are analyzed in this paper comparing the operational parameters gained during the injection of impure CO_2 (pressures, temperatures and flow ranges) with its corresponding baseline previously determined (i.e. 1500 tons of pure CO_2 were injected during the reservoir hydraulic characterization). Besides that, the geochemical reactivity analysis of impure CO_2 injected in this saline aquifer and its correlation with the results from laboratory tests were assessed.

As main conclusions from laboratory scale results, a porosity diminution was measured after the injection of CO_2 with 5%v of SO_2; apart from that, without SO_2, the effluent pH was in the range of 7–8 whereas in case of CO_2 and SO_2, a pH of 1–2 was obtained. Otherwise and focused on field scale tests, a density decrease was detected comparing the base case (pure CO_2) with the CO_2 injection containing 5.1%v of synthetic air. On the other hand, Ca^{2+}, SO_4^{2-}, Mg^{2+} and K^+ migration effects in the rock were also detected and analyzed.

1. Objective

The main objective was to carry out field scale injection tests of CO_2 and synthetic air (i.e. O_2 and N_2) into fractured carbonates with poor primary porosity and transmissivity through the fracture network, to identify and assess the impacts of these impurities in the short-term stability of CO_2 storage and their influences on site operation. Laboratory scale test campaign was previously conducted in order to study the chemical interactions between impure CO_2/brine and carbonates reservoir.

2. Introduction

Years of work culminated in the Paris Agreement in which some of the main key points were: 195 countries are involved; reduce the temperature rise to below 2 °C it is desired; the Carbon Capture and Storage (CCS) is now an accepted technology in the United Nations Framework Convention on Climate Change (UNFCCC) (Dixon and Gale, 2016; IEAGHG, 2016; Christian, 2015). CCS is recognized one of the key existing technologies to reduce the global emissions of CO2 into the atmosphere (International Energy Agency (IEA), 2013). Regarding technical aspects, this technology has "a green light" although there are some important uncertainties to be solved (Delgado et al., 2014).

Abbreviations: BHP, bottom-hole pressure; BOP, balance of plant; CCS, carbon capture and storage; CIUDEN, Fundation Ciudad de la Energía; DOT, pressure vessel used to store fluids at above atmospheric pressure, the acronym is department of transport; DTS, distributed temperature sensing; ERT, electrical tomography system; Fm, formation; FTIR, Fourier Transform Infrared (analyzer); HA well, Hontomín observation (or auscultation) well; HI well, Hontomín injection well; IEA, International Energy Agency; I&C, instrumentation and control; LoT, leak-off-test (pressure); PFD, process flow diagram; TDP, Technology Development Plant; WHP, well-head pressure.

* Corresponding author.
E-mail addresses: jc.dedios@ciuden.es, jcdediosgonzalez@gmail.com (J.C. de Dios).

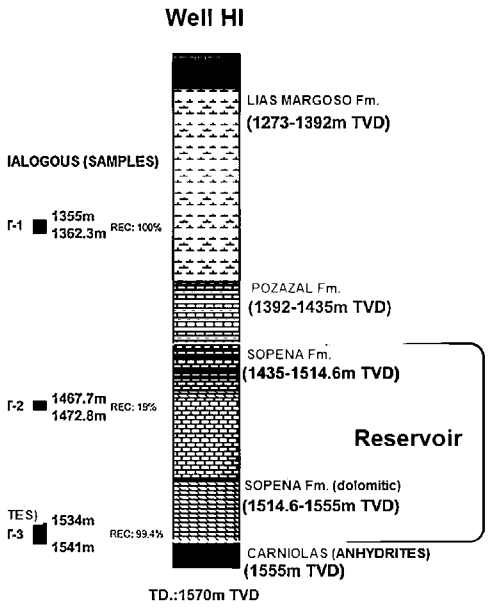

Fig. 1. Hontomín TDP formations.

Fundación Ciudad de la Energía (CIUDEN) has successfully completed the full CCS chain, being CO_2 captured in the Technology Development Centre in Cubillos del Sil (León, Spain) whereas it is geologically injected into a deep saline aquifer located in the Hontomín Technology Development Plant (TDP) (Burgos, Spain) (Fernandez et al., 2015).

Regarding CO_2 storage, one of the most important uncertainties of this technology is to understand the physico-chemical processes that take place in the rock-brine-CO_2 system within the seal-reservoir geological complex during and after CO_2 injection and, particularly, the changes induced on operational processes due to impurity effects (Brosse et al., 2005; Michael et al., 2015). CIUDENís activities are focused on this issue including the accomplishment of experiments in laboratory and field scale. It should be noted that selected impurities used in laboratory and their composition are different than in field scale case, with the aim to avoiding operations that could cause damages to the geological formations and the facility.

3. Material and methods

3.1. Hontomín TDP

Regarding the geological formations to inject CO_2 in Hontomín TDP, Sopeña Formation (Fm) was selected due to better injectivity conditions during the site hydraulic characterization. This formation presents a poor matrix porosity and permeability through the fracture network, conditioned by hydrodynamic effects induced by the injection of CO_2 and brine and the geochemical reactivity between the mixture previously specified and the reservoir rock. As it is explained in Fig. 1, Sopeña Fm. consists of two different layers: limestones and dolomites; in Table 1, Sopeña Fm. mineralogical composition is showed (Global CCS Institute, 2015).

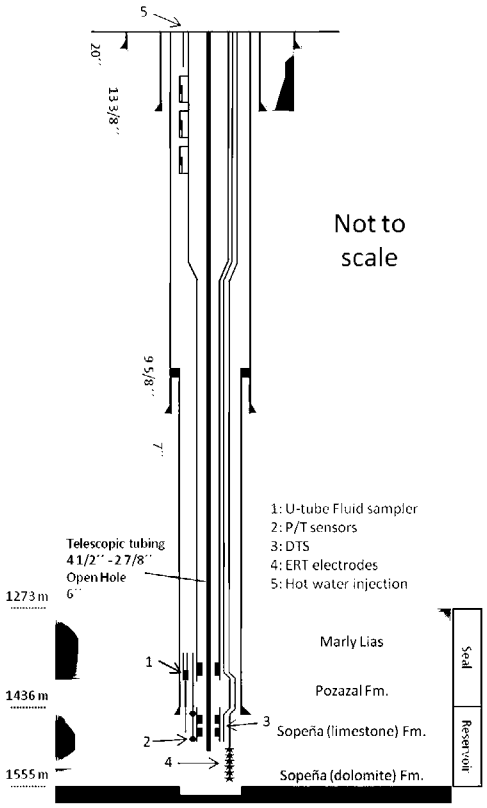

Fig. 2. X-mas tree and instrumentation of H-I well.

Otherwise, following units are installed in Hontomín TDP: injection well and observation well (hereinafter, HI and HA), CO_2 injection facility and water conditioning facility.

3.1.1. HI and HA wells (Neele et al., 2014)

HI well is equipped with the following instrumentation (also shown in Fig. 2) that it is in line with the state-of-the art (Jenkins et al., 2015):

a) Distributed temperature sensing system (DTS) for fluid temperature measurement along the injection tubing.
b) Line with 2 dual P/T sensors to measure pressure and temperature in the injection formation.
c) U-Tube fluid deep sampler.
d) 6 electrodes set for electrical tomography system (ERT), at intervals of 8 m, hanging below the steel injection tubing immersed in brine.

Highlighting that 18 linear meters of chokes are installed at 1000 m depth, in order to produce a pressure drop up to 60 barg. As shown in Fig. 2, these instrumentations cross the packer (grey area).

Regarding HA, with a distance of 50 from HI, the well is equipped with similar instrumentation than injection well (see Fig. 3):

a) P/T sensors to measure at 4 different levels in the open hole (seal and reservoir).

Table 1
Hontomín reservoir mineralogy.

	Limestone (% w)	Dolomite (% w)	Anhydrite (% w)	Other
Sopeña limestone unit	97	3	0	Dolomite grainstone intercalations
Sopeña dolomite unit	0	98	2	–

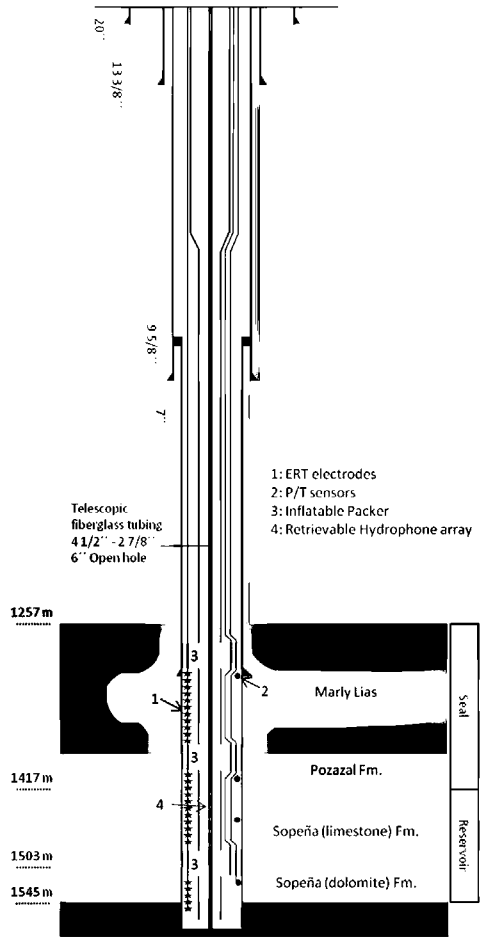

Fig. 3. X-mas tree and instrumentation of the H-A well.

b) 28 electrodes for electrical resistivity tomography (hereinafter, ERT) installed at intervals of 7–8 m.
c) Mobile hydrophones spaced regularly at intervals of 9 m.

Also worth mentioning is the U-tube operating principle due to the important role of this deep sampler during the test campaign conducted on site. The U-tube is a simple positive fluid displacement pump which uses a high pressure gas drive (Freifeld, 2009). Its core is the ball check-valve installed at the top of the hydraulic packer (1428 m depth), and below it, the inlet filter and thin tubing which reaches the bottom hole. This valve contains the only moving part of the system in the borehole. A loop of tubing, with the "sample leg" and "drive leg" as it is shown in Fig. 4, reaches the surface for extracting deep fluid samples. Check-valve is located below a "tee" at the base of the U and permits the fluid to enter into the loop, closing (by application of gas from the surface) when the pressure in the U is increased above the hydrostatic value. The inlet, below the check-valve to prevent the plugging, is manufactured by a sintered stainless steel filter.

For collecting a sample (Freifeld, 2009), once the check valve is open, the U is firstly filled by venting and driving the fluid from the reservoir to the inside of both legs. At this stage the check valve is closed and the sample is recovered by supplying high-pressure N_2 through the drive leg, enhancing the fluid recovery through the sample leg.

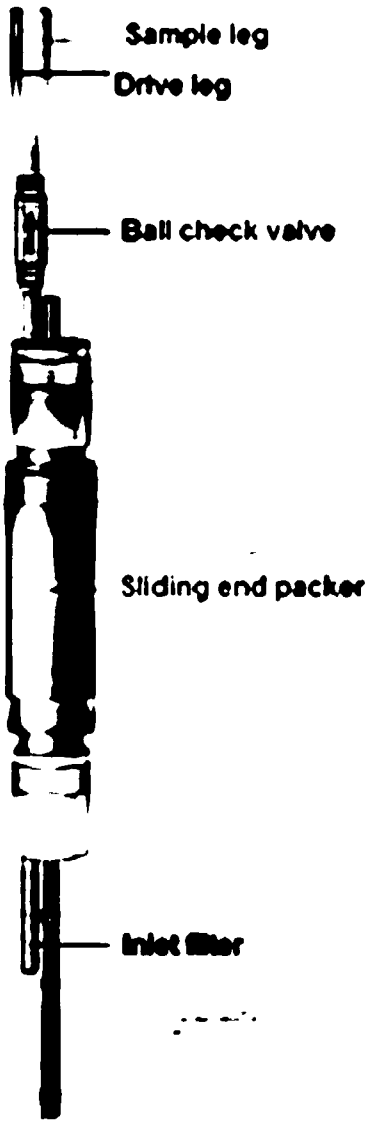

Fig. 4. U-tube scheme.

3.1.2. CO_2 injection facility

This facility is formed by three cryogenic tanks (50 tons each one), injection pumps, CO_2 heater/gasifier, balance of plant (BOP) and instrumentation and control (I&C) parts.

In order to monitor the synthetic air injection, four different cylinder racks were used in parallel (see *TRACING/DOPPING AREA* in) Fig. 5. For acquiring representative data to quantify the amount of synthetic air that was injected in the main CO_2 stream during each test, one of the four cylinders rack was located over a scale to provide information which could corroborate the measurements gained from the facility monitoring.

After the injection tests, samples from the borehole were extracted using the U-tube device on a weekly basis, considering a period of three months. Taking into account that the samples were extracted in "reservoir conditions" (pressure and temperature), they were analyzed in two steps:

- Step #1 or gas phase analysis: It was performed using a Fourier Transform Infrared analyzer (FTIR) (see Table 2).
- Step #2 or liquid phase analysis: It was conducted in two different equipments: the ion chromatography and the carbonate analyzer. In the first case, the determination of anions and cations were

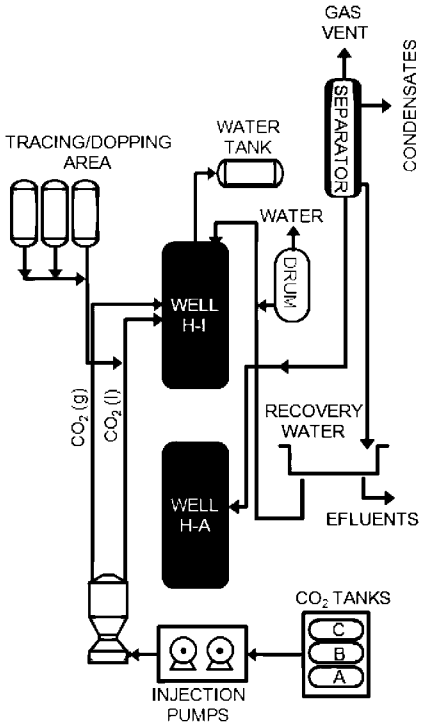

Fig. 5. Schematic process flow diagram (PFD) of Hontomín TDP.

Table 2
Technique and equipment model used during the field tests.

Technique	Equipment Model or Supplier
Multigas Infra Red Fourier Transform analyzer	Environnement S.A. (Environnement S.A.)
Ion-exchange chromatograph	METROHM model automatic processor 850 professional IC (METRHOHM)
Carbonate analyzer	CO-202 designed by EQUILAB (EQUILAB)

done (in particular: Cl^-, SO_4^{2-}, Na^+, Mg^{2+}, Ca^{2+}, F^-, Br^-, Li^+, K^+). On the other hand, the total CO_2 dissolved in the liquid samples was measured in the carbonate analyzer.

3.2. Laboratory equipments

CIUDEN performed surface campaigns collecting cores from outcrops (analogues) corresponding to the caprock and reservoir, being used in the laboratory tests.

Generally speaking, the laboratory tests were based on the injection of a CO_2 stream with and without impurities in Hontomín analogues according to the following methodology:

- Measurements before the injection:
  - Mass, helium porosity and gas permeability measurement.
- Analogue saturation with sodium chloride (NaCl) with a concentration of 40 g/l and determining its permeability by CORETEST equipment.
  - The analogue is covered with a thermo-retractable plastic in its lateral area.
  - Set the conditions of the experiment.
  - Inject pure CO_2 or impure CO_2 throughout the cores. The total volume injected was, at least, higher than 5 times the porous volume of the sample.
  - The test duration was five days (8 h/day).
- Measurements after the injection:
  - Mass, helium porosity and gas permeability measurement.

Table 3
Technique and equipment model used during the laboratory tests.

Technique	Equipment Model
Mercury porosimetry	QUANTACHROME (POREMASTER 60GT) (QUANTACHROME)
Gas permeameter	VINCI Technologies GasPerm (VINCI Technologies)
Un-steady state Relative Permeability System	CORETEST SYSTEMS RelPerm (CORETEST SYSTEMS INC.)
Ion-exchange chromatograph	METROHM model automatic processor 850 professional IC (METRHOHM)

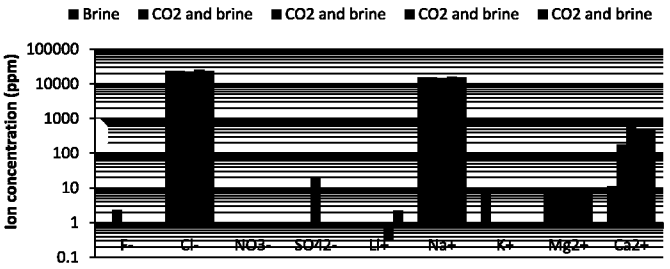

Fig. 6. Ion concentration for effluents produced during the test (sample B1.4.2).

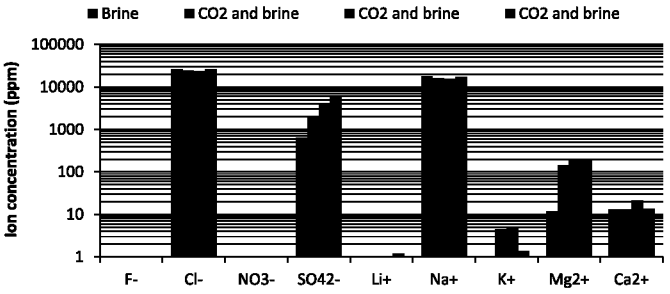

Fig. 7. Ion concentration for the effluent produced during the test (sample B1.3A).

- Ion chromatography of effluents generated during NaCl saturation and the injection tests.

Worth mentioning the requirements of the samples in order to do these tests were: Porosity ≥5%; permeability >1 mD; diameter: 1,5″; length: 1–3″. Regarding the procedure basis, Table 3 shows the technique and equipment used for these tests:

4. Results

4.1. Laboratory scale tests

The test matrix is included In Table 4; a comparison between the injection of pure CO_2 and CO_2 containing SO_2 was selected as the case study in laboratory scale. As explained above, it is needed to remind that the selected impurity (SO_2) and the composition of the mixtures used in laboratory were different than the used in the field scale tests, in order to avoid some damage that could be caused to the reservoir and/or the facility.

Based on the steps related in the Chapter 3.2, the following tables (Tables 5–8) show the results gained from each sample considered in the test matrix.; the Figs. 6 and 7 are the representation of the data included in Tables 6 and 8.

4.2. Field scale results

4.2.1. Composition of injection stream

Considering the quantity of synthetic air (kg/min) that was injected in each test, the real composition of CO_2 stream was cal-

Table 4
Laboratory scale test matrix.

Type of experiment	Sample type	Sample name	CO_2 impurity	Concentration of CO_2 impurity	P-T conditions	Brine	Brine concentration
Plug Flow (dynamic tests)	Sopeña limestone	B1.4.2	Pure CO_2	0%	150 bar/50 °C	NaCl	40,00 ppm
		B1.3A	CO_2 + SO_2	5%			

Notes: The values presented correspond with the main characteristics of Hontomín TDP.

Table 5
Physical properties for the sample B.1.4.2 before and after CO_2 injection.

	Before	After
L (mm)	42.32	42.32
D (mm)	37.19	37.19
m (g)	101.67	100.27
Φ (%)	18.87	21.02

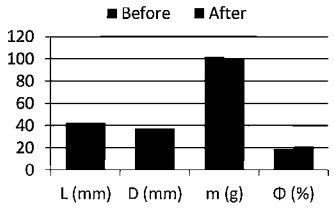

Notes: L = length, D = diameter, m = mass (dry basis), Φ = porosity.

Table 6
Ion concentration for effluents produced during the test (sample B1.4.2).

Sample name	Liquid sample	Cycle	Anion Concentration (ppm)			Cation Concentration (ppm)					pH	Cond (mS/cm)
			F^-	Cl^-	SO_4^{2-}	Li^+	Na^+	K^+	Mg^{2+}	Ca^{2+}	–	–
B1.4.2	1	Brine	0	23,605	0.0	0.9	15,389	8.1	9.9	11.3	7.0	60.9
	2	CO_2 and brine	2.3	23,868	0.0	1.0	15,631	0.0	8.7	178.1	7.6	61.4
	3	CO_2 and brine	0	22,560	19.9	0.9	14,768	0.0	9.0	547.2	7.1	57.5
	4	CO_2 and brine	0	25,001	0.0	0.3	16,352	0.0	9.2	508.3	7.5	63.3
	5	CO_2 and brine	0	23,223	0.0	2.2	15,221	0.0	10.2	519.5	7.1	59.8

Table 7
Physical properties for the sample B.1.3A before and after CO_2+SO_2 injection.

	Before	After
L (mm)	46.23	46.23
D (mm)	37.29	37.29
m (g)	116.77	115.83
Φ (%)	8.94	1.95

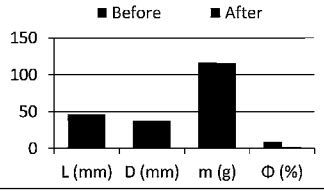

Notes: L = length, D = diameter, m = mass (dry basis), Φ = porosity.

Table 8
Ion concentration for the effluent produced during the test (sample B1.3A).

Sample name	Liquid sample	Cycle	Anion Concentration (ppm)			Cation Concentration (ppm)					pH	Cond (mS/cm)
			F^-	Cl^-	SO_4^{2-}	Li^+	Na^+	K^+	Mg^{2+}	Ca^{2+}	–	–
B1.3A	1	Brine	0,0	25.757	628,4	0,0	17.516	0,0	11,83	13,3	8,66	64,7
	2	CO2 and brine	0,0	24.303	1.961	0,0	16.013	4,5	144,1	13,1	1,75	64,8
	3	CO2 and brine	0,0	23.829	4.062	0,0	15.692	4,8	182,9	21,6	1,2	66,8
	4	CO2 and brine	0,0	26.018	5.700	1,2	17.144	1,4	194,8	13,4	0,98	74,2

culated. For the case study considered in this manuscript, in which a theoretical value of 5%v of air should have been injected, a time-averaged value of 5.1%v was really injected (see Fig. 8)

As the Reader can check, in some specific periods (around 13:15 h) the quantity of injected air was higher than the averaged value due to the operational effects of cylinder rack changes; however, this effect has to be considered as a transient period that did not have influence in the test regarding total pipeline length (ca. 1700 m considering pipe and injection tubing).

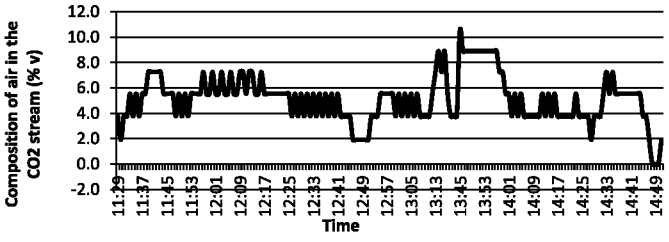

Fig. 8. Real composition of air in the CO_2 stream.

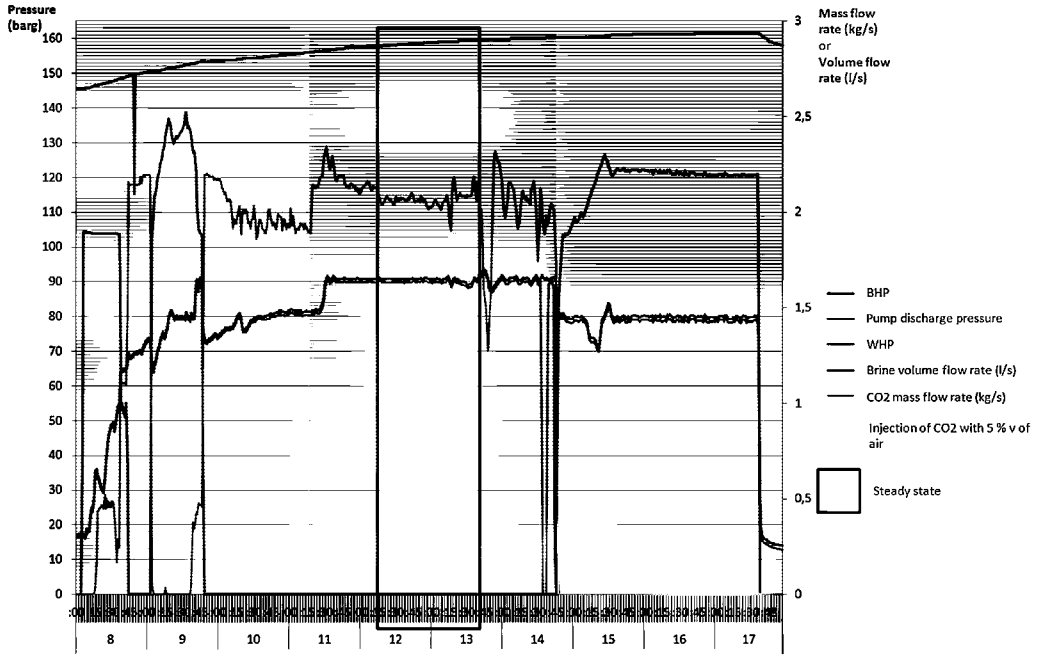

Fig. 9. Main operational parameters during the injection of impure CO_2.

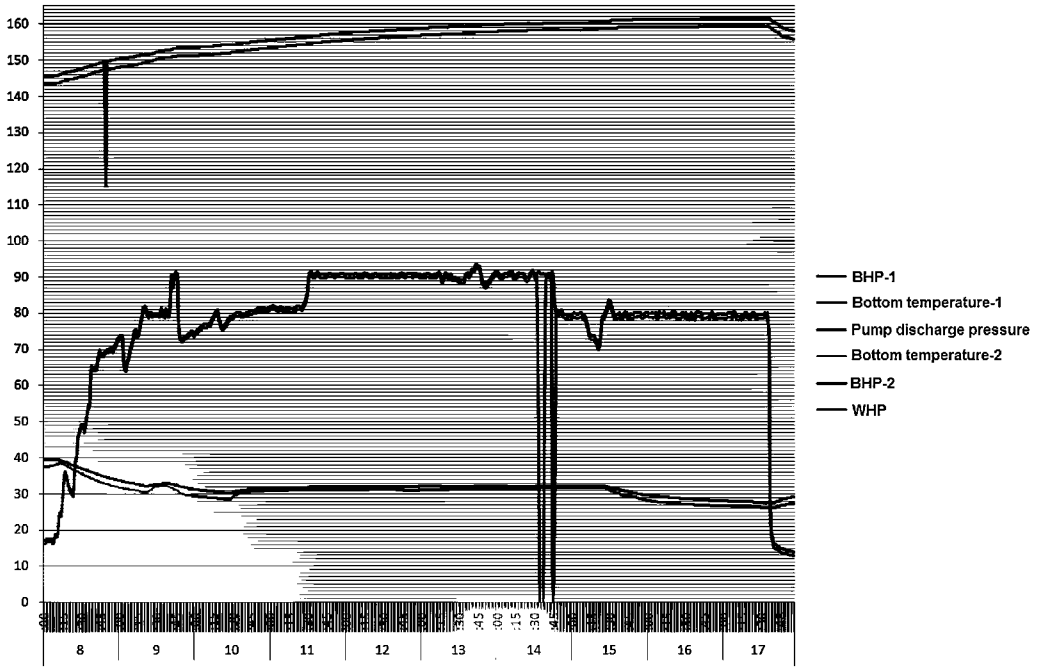

Fig. 10. Injection of CO_2 in supercritical conditions.

4.2.2. Operation parameters

4.2.2.1. Injection regime and wellhead vs bottom-hole pressure. During the injection of 5.1%v of synthetic air, following results were gained as Fig. 9 shows:

4.2.2.2. Storage conditions. Fig. 10 among other parameters, pressure and temperature at the bottom hole are represented to corroborate that CO_2 was stored in supercritical conditions into the reservoir. Taking into account the values of these parameters on the well head (see previous Fig. 9) it is needed to monitor the temperature along the tubing for assessing the injection conditions.

4.2.3. Differential pressure in the bottom hole

Regarding the information given in Fig. 2, two pressure transmitters are installed in the injection bottom hole, being the distance between them of 25 m.

The measured pressure values allowed calculation of fluid density using the hydrostatic pressure equation. Consequently, two different graphs are plotted: first graphic shows the differential pressure and the density calculated during the injection of pure CO_2 (Fig. 11) whereas in a second block of figures, it is represented the comparison of calculated densities between the base case (pure CO_2) and CO_2 containing 5.1%v of air, concluding that density value

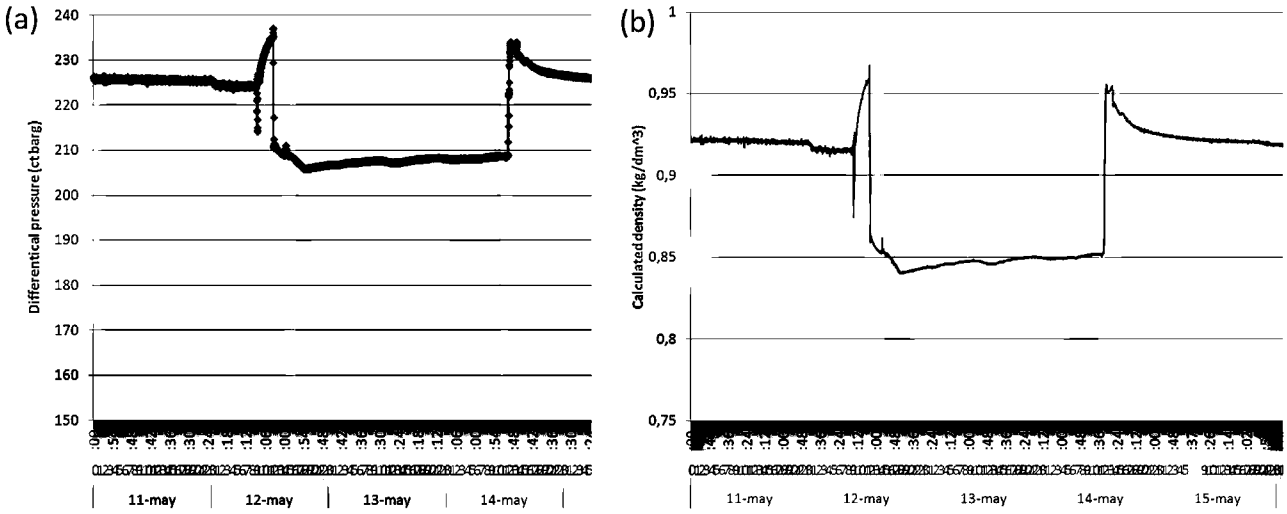

Fig. 11. (a) Differential pressure and (b) density calculated during the injection of pure CO_2.

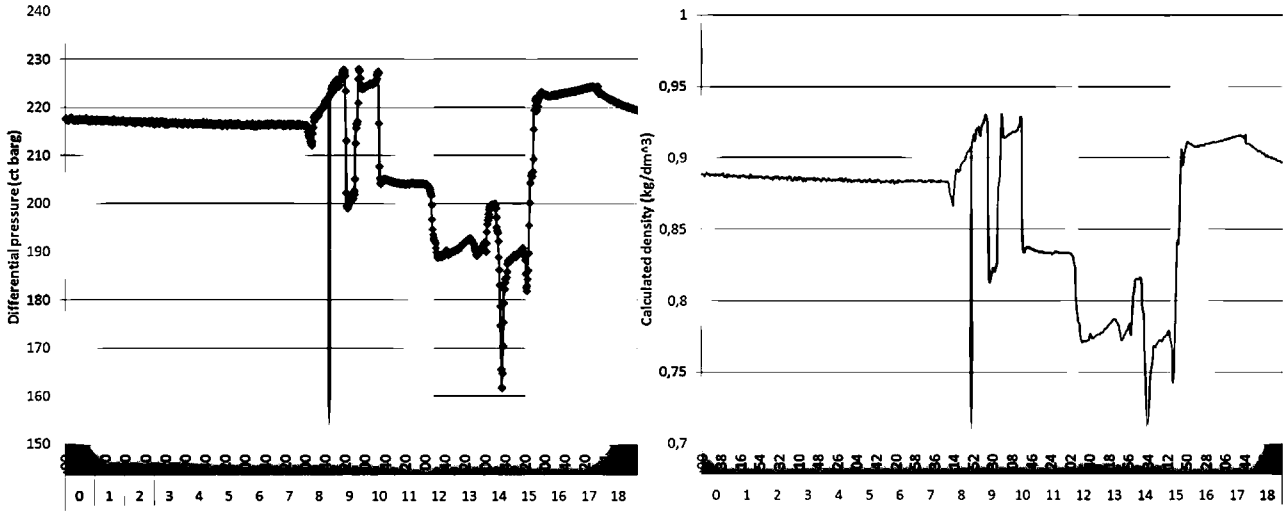

Fig. 12. Comparison between the calculated density values for the pure CO_2 and the CO_2 with 5.1%v of air.

decreases from 840 kg/m^3 to 775 kg/m^3 in reservoir conditions (Fig. 12).

4.2.4. Temperature monitoring along injection tubing

Distributed Temperature System (DTS) is a device used to monitor the temperature evolution along the injection tubing (Jenkins et al., 2015). In Fig. 13, the results from the Distributed Temperature Sensing (DTS) are showed for three different stages: formation water, pure CO_2 injection and CO_2 with synthetic air (5.1%v) injection.

A perturbance is produced close to 1000 m depth, as it is shown in Fig. 13; the reason was that 18 linear meters of chokes were installed inside the injection tubing at this depth to generate a pressure drop for avoiding to reach values higher than the Leak-of-test pressure (LoT) of reservoir formation (Birkholzer et al., 2015; Bachu, 2015) with the consequent negative effects such as induced seismicity in surface and leakages affecting potable groundwater resources (Jones et al., 2015; Birkholzer et al., 2015). A temperature decrease is generated as well, due to the Joule-Thomson effect, as consequence of the fast CO_2 expansion at the choke outlet (Fig. 13).

According to the data gained during the CO_2 injection in the well head (Fig. 9), the bottom hole (Fig. 10) and the DTS, it can be assured that the injection was performed in liquid-phase along the tubing. Consequently, the coupling between well head pressure (WHP) and bottom hole pressure (BHP) due to monophase flow conditions during injection was confirmed.

4.2.5. DOTs[1] gas phase analysis

Figs. 14 and 15 represent the results obtained for the gas phase from the tests performed by pressure vessels used to store fluids at above atmospheric pressure (DOTs) (see step #1 previously explained in the Chapter 3.1.2).

After the injection of impure CO_2, different extractions were carried out in order to analyze the reservoir behaviour after the injection of CO_2 with the impurity of 5.1%v of air (see step #1 explained in the Chapter 3.1.2); analogously to the base case previously presented, following figures (Figs. 16 and 17) represent the results obtained for the gas phase.

4.2.6. DOTs liquid phase analysis

Fig. 18 represents the composition of CO_2 in the liquid phase for different samples, i.e. the quantity of CO_2 dissolved at atmospheric pressure (see step #2 previously explained in the Chapter 3.1.2)

[1] DOT is a pressure vessel used to store fluids at above atmospheric pressure.

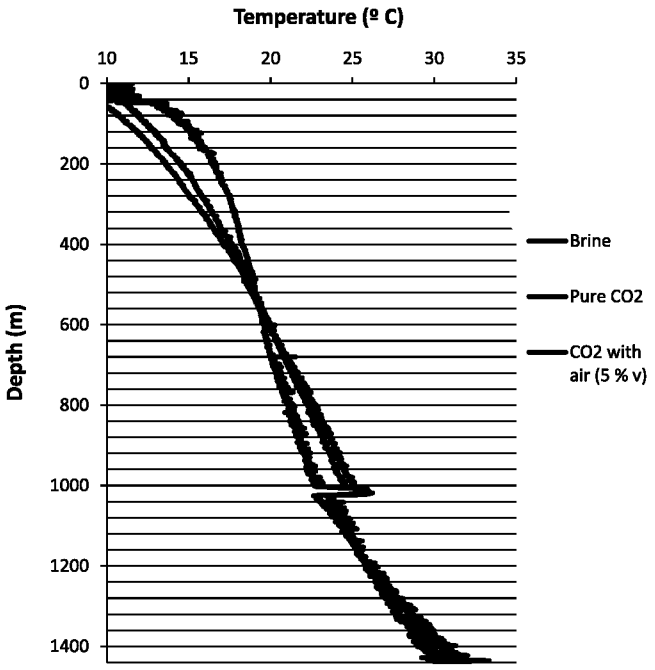

Fig. 13. Temperature profile along the injection tubing in HI well at Hontomín TDP for three different stages: Formation water, pure CO_2 injection and CO_2 with synthetic air injection.

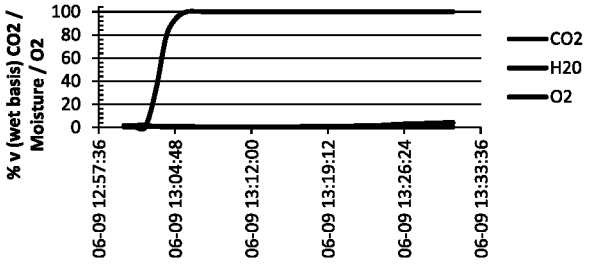

Fig. 14. Major components (%v) measured in the gas phase after the injection of pure CO_2.

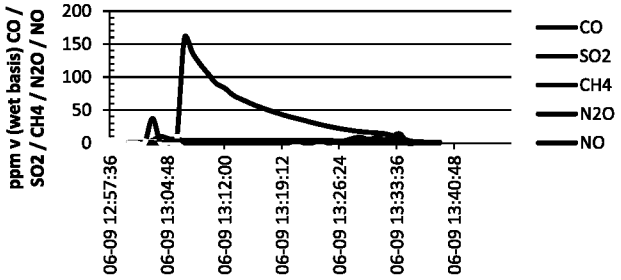

Fig. 15. Minor components (ppmv) measured in the gas phase after the injection of pure CO_2.

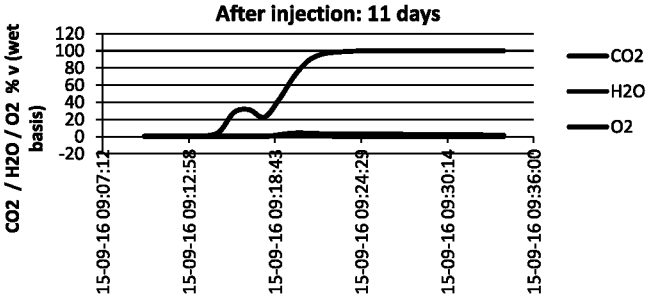

Fig. 16. Major components (%v) measured in the gas phase after the injection of impure CO_2.

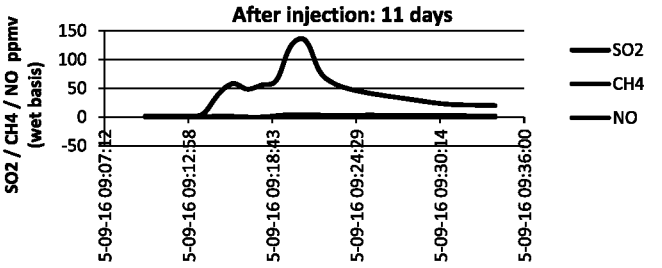

Fig. 17. Minor components (ppmv) measured in the gas phase after the injection of pure CO_2.

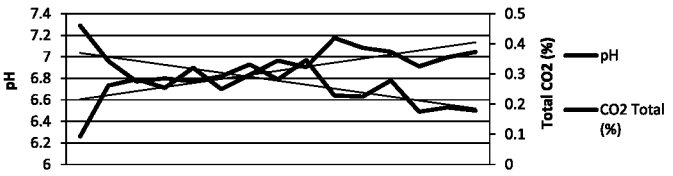

Fig. 18. CO_2 dissolved in the liquid phase at atmospheric pressure.

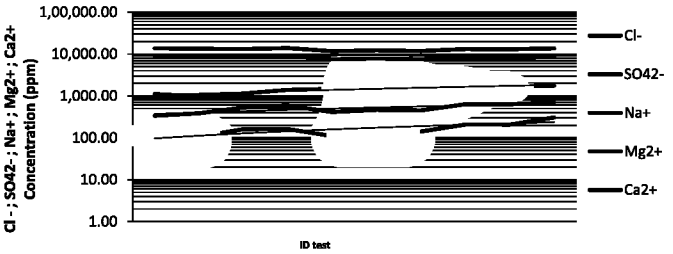

Fig. 19. Ion chromatography results for the major component in the liquid phase (for all the samples).

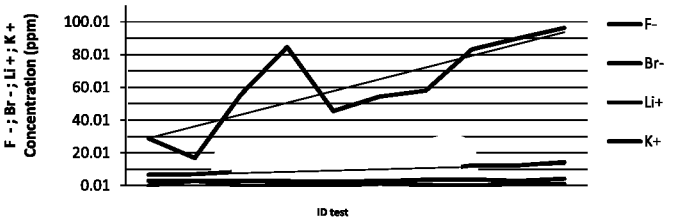

Fig. 20. Ion chromatography results for the minor component in the liquid phase (for all the samples).

whereas Figs. 19 and 20 represent the ion composition (anions and cations) in the liquid phase (the first graph indicates the major components whereas the second presents the minor ions).

5. Discussion

Carbon dioxide sequestered will be trapped by physical and chemical processes. Focusing on chemical trapping, a distinction between aqueous phase trapping (solubility and ionic trapping) and mineral trapping can be done (Talman, 2015). Considering the duration of the test, it is clear that the second case is not the scope of this work so only the expected reaction with the aqueous phase should be taken into account, i.e. solubility of water in the injected high-density CO_2^- stream and hydrolysis reactions or ionization of water (Talman, 2015):

$$CO_2\,(aq) + H_2O \leftrightarrow H^+ + HCO_3^-$$

$$CO_2\,(aq) + H_2O \leftrightarrow 2H^+ + CO_3^{2-}$$

Several trace impurities also undergo hydrolysis reactions; these are H_2S, SO_2 and NH_3; considering the scope of this work, SO_2 is included in this section with a higher degree of detail. SO_2 forms the strongest acid, it will protonate HCO_3^- to form CO_2 (aq).

Regarding the laboratory results previously described, if we compare the values of porosity between the injection of pure CO_2 and CO_2 with 5.1%v of SO_2, in the second case, the result was much lower (≈80%). In our opinion this effect could have two possible causes: first hypothesis is the samples were extracted from the pressure chamber suffering both fast cooling and expansion at the end of each test, and consequently, the Cl^- and Na^+ precipitated into the rock matrix with the final diminution of porosity; other possibility is based on the fact that due to the high concentration of SO_2 (5.1%v is not common in flue gases to be captured (Global CCS Institute, 2014)), the porosity was decreased due to the precipitation reactions such as the carbonate andsulphate formations. This last hypothesis should be studied deeply in future longer laboratory tests.

Focused on the field scale tests, DTS monitors the temperature evolution along the injection tubing. At this point, it was obtained that higher the concentration of air in the CO_2 stream, higher is the Joule-Thomson effect (i.e. diminution of the temperature with the variation of pressure). As a future work, these measurements have to be compared with the theoretical values provided by TREND software (Span, 2015).

Finally, it is needed to highlight that during the following 11 days after the injection of impure CO_2, the gas phase samples gained were the same nature as the base case (i.e. injection of pure CO_2). At this point, Reader is reminded that 150 t of impure CO_2 were injected, and in our opinion that quantity was not enough to achieve clear results for determining how the reservoir behaviour is in terms of structural trapping at Hontomín site.

6. Conclusions

In this work, experiments on laboratory and field scale have been performed to study physical and chemical interactions in the short term between CO_2 and impurities, brine and reservoir rock, in order to assess their influence in a safe and efficient injection and the implications involved for the CO_2 geological storage.

Focused on the laboratory scale, dynamic tests (samples are located in a liquid permeameter where the CO_2 flows through the sample) of analogous from Hontomín reservoir have been done; 150 barg and 45 °C were planned as P and T conditions (Hontomín reservoir conditions) and SO_2 was selected as impurity considering a concentration of 5.1%v in the CO_2 stream. As main conclusions, a sample negligible mass diminution (around 1%) was measured after the injection, independently of the degree of impurity; regarding the porosity, it was much lower (≈80%) after the injection of CO_2 with 5%v of SO_2. Besides that, other important differences detected are the effluent pH and the ion migration phenomena. In regards the pH value, for the pure CO_2 injection tests the effluent pH was in the range of 7–8 but if impure CO_2 was injected, the pH obtained was in the range of 1–2 (Pearce et al., 2015). Regarding the second effect with the mixture of CO_2 and SO_2, chemical modifications were detected, being mainly based on the modification of Mg^{2+} and SO_4^{2-} due to migration phenomena produced by the acidification previously explained.

The short-term co-injection of CO_2 and synthetic air (i.e. O_2 and N_2) field scale tests were conducted in order to identify the impact of these impurities in the reservoir behaviour of Hontomín Technology Development Plant. For a synthetic air concentration of 5.1%v and based on the pressure and temperature at the bottom injection well (158 barg, 31 °C), it was possible to assure that the CO_2 is stored in supercritical conditions at Hontomín reservoir. On the other hand, DTS data reveal that the injection is performed in monophase flow (liquid). Consequently, the coupling between WHP and BHP due to single phase fluid conditions during injection was also confirmed.

It was possible to calculate the fluid density using the two pressure transmitters installed at the bottom of the injection well and considering the distance between these two devices. Comparing the base case (pure CO_2) with the case of CO_2 containing 5.1%v of air, the density decreases from 840 kg/m^3 to 775 kg/m^3 at the storage conditions (i.e. 8% of diminution in the density). Consequently, the storage capacity of the reservoir suffers an impact due to the replacement of CO_2 but also due to the mixture of CO_2 and impurities do not compress to as great a degree as CO_2.

Otherwise, regarding the operation conditions showed in Fig. 9, the well head pressure needed to inject the mixture of CO_2 and 5.1%v of air, increased from 80 bar, corresponding to the case of pure CO_2, to 90 bar. That effect reveals that the higher value of WHP is due to the need to inject a mixture of CO_2 in liquid phase with the impurities (N_2 and O_2) in gas phase. By the foregoing, we can conclude that the injection of N_2 and O_2 in concentrations of 5.1%v of air (79% N_2 and 21% O_2) is less efficient than the injection of pure CO_2.

Several fluid samples from the borehole were extracted using the U-tube. Taking into account that each sample was extracted at the same conditions as the borehole (high pressure and temperature), the gas and the liquid phases were analyzed separately. Regarding the first analysis (gas phase), following main compounds were detected: NO, SO_2, CH_4 and CO_2.The composition of these compounds is showed in Table 9:

Table 9
Main components identified in the DOT gas phase.

Compound	Composition
NO	40 ppm
SO_2	10 ppm
CH_4	160 ppm
CO_2	100%

For the case of liquid phase, apparently there were more ions in the brine after the injection of CO_2 (base case), brine (operational reasons) and impure CO_2. In particular, Ca^{2+}, SO_4^{2-}, Mg^{2+} and K^+ concentration were increased. This may be due to ion migration effects in the rock according to test duration and the nature of the impurities (O_2 and N_2), no were detected (Talman, 2015). Finally and continuing with the liquid phase analysis, worth mentioning is the fact that the dissolved CO_2 trend is positive although the test durations were not enough (there is more CO_2 dissolved conform over time) whereas the pH behaviour is the contrary (negative trend).

Acknowledgments

The research leading to these results has received funding from the European Community's Seventh Framework Programme (FP7-ENERGY-20121-1-2STAGE) under grant agreement no. 308809 (The IMPACTS project). The authors acknowledge the European Commission, Spanish Government through Fundación Ciudad de la Energía (CIUDEN), project partners and the following funding partners for their contributions: Statoil Petroleum AS, Lundin Norway AS, Gas Natural Fenosa, MAN Diesel & Turbo SE and Vattenfall AB, without which this project would not have been completed successfully

The sole responsibility of this publication lies with the authors. The European Union is not responsible for any use that may be made of the information contained therein.

References

Bachu, S., 2015. Review of CO2 storage efficiency in deep saline aquifers. Int. J. Greenh. Gas Control 40, 188–202.

Birkholzer, J.T., Oldenburg, C.M., Zhou, Q., 2015. CO2 migration and pressure evolution in deep saline aquilfer. Int. J. Greenh. Gas Control 40, 203–220.

Brosse, E., Magnier, C., Vincent, B., 2005. Modelling fluid-rock interaction induced by the percolation of CO2-enriched solutions in core samples: the role of reactive surface area. Oil Gas Sci. Technol. 60, 287–305.

CORETEST SYSTEMS INC., RPS-Series Relative Permeability Systems, [Online] Available: http://www.coretest.com/rps-series-relative-permeability-systems.html (accessed 01.02.16.).

Christian, B., 2015. EuroActiv, 01 2015 [Online]. Available: http://www.euractiv.com/sections/energy/capture-carbon-311149.

Delgado, M.A., Diego, R., Alvarez, I., 2014. CO2 balance in a compression and purification unit (CPU). Energy Procedia, 322–331.

Dixon, T., Gale, J., COP-21 and the Paris Agreement, 2016.

EQUILAB, EQUILAB CO-202 Benchtop Carbonates Analyzer, [Online]. Available: http://www.equilab.es/co202.html (accessed 02.03.16.).

Environnement S.A., Multi-gas Infra Red Fourier Transform (FTIR) Analyzer, [Online]. Available: http://www.environnement.it/public/articoli/64/files/mirft_uk_s_p.pdf (accessed 28.02.16.).

Fernandez, D., De Dios, J.C., Marin, J., 2015. Hydraulic characterization tests at Hontomin technology development plant for CO2 storage. Experiences with brine, CO2 and tracer injection. In: Trondheim CCS Conference, Trondheim, 2015.

Freifeld, B., 2009. The U-tube: a new paradigm for borehole fluid sampling. Sci. Drill. 8 (September).

Global CCS Institute, 2014. The Global Status of CCS February 2014. Global CCS Institute.

Global CCS Institute, 2015. Hontomin Reservoir Characterization Tests.

IEAGHG, Greenhouse News – The official newsletter of IEAGHG and its members, 28.03.2016 [Online]. Available: http://ieaghg.org/.

International Energy Agency (IEA), 2013. Technology Roadmap: carbon capture and storage.

Jenkins, C., Chadwick, A., Hovorka, S., 2015. The state of the art in monitoring and verification – ten years on. Int. J. Greenh. Gas Control 40, 312–349.

Jones, D., Beaubieny, S., Blackford, J., 2015. Developments since 2005 in understanding potential environmental impacts of CO2 leakage from geological storage. Int. J. Greenh. Gas Control 40, 350–377.

METRHOHM, Intelligent Ion Chromatography, [Online]. Available: http://www.mep.net.au/wpmep/wp-content/uploads/2013/07/M770_MEP_IC-914503_88505007EN.pdf (accessed 28.01.16.).

Michael, K., Golab, A., Shulakova, V., Ennis-King, J., Allinson, G., Sharma, S., Aiken, T., 2015. Geological storage of CO2 in saline aquifers – a review of the experience form existing storage operations. Int. J. Greenh. Gas Control 4, 659–667.

Neele, F., Quinquis, H., Read, A., 2014. CO2 storage development: status of the large European CCS projects with EEPR funding. Energy Procedia 63, 6053–6066.

Pearce, J., Law, A., Dawson, G., Golding, S., 2015. SO2-CO2 and pure CO2 reactivity of ferroan carbonates at carbon storage conditions. Chem. Geol. 411 (September), 112–124.

QUANTACHROME, POREMASTER Series. Automated Mercury Porosimeters, [Online]. Available: http://www.quantachrome.com/pdf_brochures/07128.pdf (accessed 10.02.16.).

Span, R., 2015. Thermophysical Properties for Transport and Storage of CO2-rich mixtures – Contributions by IMPACTS, Athens.

Talman, S., 2015. Subsurface geochemical fate and effects of impurities contained in a CO2 stream injected into a deep saline aquifer: what is known. Int. J. Greenh. Gas Control 40, 267–291.

VINCI Technologies, Steady state gas permeameter (Gasperm), [Online]. Available: http://www.vinci-technologies.com/ (accessed 15.12.15.).